Journal of Alloys and Compounds 997 (2024) 174827

Contents lists available at ScienceDirect

Journal of Alloys and Compounds

journal homepage: www.elsevier.com/locate/jalcom

Construction of unary and ternary ZnO–CuO–CdO composite thin films and comprehensive analysis of their optical, electrical, and photocatalytic performance

Osman Kahveci [a], Abdullah Akkaya [b], Ebru Karakaş Sarıkaya [c], Murat Çanlı [b], Raşit Aydın [d,*], Bünyamin Şahin [c,e], Enise Ayyıldız [a,f]

[a] Department of Physics, Faculty of Sciences, Erciyes University, Kayseri, Turkey
[b] Mucur Technical Vocational Schools, Tech. Prog. Department, Kırşehir Ahi Evran University, Kırşehir, Turkey
[c] Department of Basic Sciences, Faculty of Engineering, Necmettin Erbakan University, Konya, Turkey
[d] Department of Physics, Faculty of Sciences, Selçuk University, Konya, Turkey
[e] BITAM-Science and Technology Research and Application Center, Necmettin Erbakan University, Konya, Turkey
[f] Energy Conversation Research and Application Center, Erciyes University, Kayseri, Turkey

ARTICLE INFO

Keywords:
Ternary oxides
ZnO-CuO-CdO
Bandgap
Photocatalytic activity
TLM method

ABSTRACT

In this study, unary ZnO, CuO, CdO, and ternary ZnO–CuO–CdO metal oxide thin film materials were fabricated using the SILAR procedure. The XRD spectra of the synthesized films show sharp and dominant diffraction lines, indicating the high crystallinity of both the unary and ternary composite films. The crystallite size values of unary ZnO, CuO, CdO, and ZnO–CuO–CdO ternary films were found to be 18.71 nm, 12.86 nm, 15.88 nm, and 21.96 nm, respectively. FESEM pictures exhibited that nanocomposites have spherical and nanorod-like hybrid morphology, and EDX showed that Cd has a higher content than Zn and Cu. The prepared samples' FT-IR spectra in the wavenumber range of 500–4000 cm^{-1} revealed the existence of numerous vibrational modes. The optical bandgap values were found to be 1.47, 3.20, 2.21, and 2.51 eV for the CuO, ZnO, CdO, and ternary ZnO-CuO-CdO films, respectively. The photocatalytic efficiency of the ternary composites is higher than that of the unary metal oxides. The specific contact resistivity values were 780.83 $k\Omega cm^2$, 213.33 $k\Omega cm^2$ 347.33 Ωcm^2, and 1.97 $k\Omega cm^2$ for ZnO, CuO, CdO, and ternary ZnO–CuO–CdO thin films, respectively. Our inventions provide advanced prompting for constructing new types of catalysts. The characterization results imply that the ternary nanocomposite can be used as a cost-effective alternative material for optoelectronic and photocatalytic implementations.

1. Introduction

Metal oxide (MO) nanocomposites (NC) have gained significant attention in recent years because of their unique properties, including electrical, mechanical, optical, thermal, structural, and photocatalytic properties [1–3]. Because of their dynamic potential, simplicity of production, size, form, and ability to be doped with different elements, nanocomposites can be used to improve the characteristics of other materials. When two or more MOs are combined on a nanoscale, NCs are created, and the characteristics of these mixtures depend on the concentration of each individual MO component. The characteristics of separate MOs have been greatly enhanced by combining them to generate unique NCs, providing a new line of inquiry for electrical, photocatalysis, biological, and optoelectronic applications [4–7].

Zinc oxide (ZnO) is a semiconductor oxide material with a direct band gap of 3.37 eV, an excitonic binding energy of 60 meV, and a high piezoelectric constant. It is classified as the n-type. ZnO is a viable option because of its low cost, biocompatibility, excellent stability, low toxicity, and environmental harmlessness. These properties make it suitable for various applications such as light emitting diodes, optically pumped lasers, biosensors, UV photoelectric devices, piezoelectric nanogenerators, and solar cells in different fields [8–11]. With a narrow optical bandgap of 1.5 eV, copper oxide (CuO) is a significant p-type semiconductor at room temperature. When compared to other materials, CuO is a cost-effective and non-toxic material that has inspired both science and industry. CuO has drawn attention because of its excellent

* Corresponding author.
E-mail address: raydin@selcuk.edu.tr (R. Aydın).

https://doi.org/10.1016/j.jallcom.2024.174827
Received 20 March 2024; Received in revised form 5 May 2024; Accepted 11 May 2024
Available online 13 May 2024
0925-8388/© 2024 Elsevier B.V. All rights are reserved, including those for text and data mining, AI training, and similar technologies.

pseudo capacitance behavior, simplicity of production at the nanoscale level, and elemental abundance [12,13]. Although cadmium is a toxic element, the oxide phase (CdO) is quite stable, like other metal oxides. CdO is a technologically important material because of its good electrical conductivity, high optical transparency, and high carrier concentration due to the natural point defects at cadmium interstitials and oxygen vacancies. With a direct band gap of 2.2–2.7 eV, CdO is a potential II–VI composite n-type semiconductor material. Owing to its low electrical resistivity, ease of doping, natural abundance, and chemical stability, CdO has attracted a lot of interest lately [14,15].

Numerous scientists have prepared ZnO, CuO, and CdO MOs, both individually and as binary nanocomposites, and studied their physical properties and photocatalytic activities. Sankaran and Kumaraguru [16] fabricated CuO/ZnO and CuO/CdO NCs using a two-step process that involved co-precipitation and hydrothermal techniques. The degradation efficiency of RhB and MG dyes was investigated using CuO/ZnO and CuO/CdO NC at room temperature. ZnO/CuO NC was synthesized by Mubeen et al. [17] using a wet chemical process. The photocatalytic activity of the samples was evaluated by testing their ability to degrade methylene blue (MB) under visible irradiation. This study reported on tuning the band structure of ZnO/CuO NCs to enhance their photocatalytic activity. Sirohi et al. [18] prepared CdO– ZnO NC using the hydrothermal method. This study demonstrated that these composites can serve as effective photocatalysts for the degradation of MB, RhB, and methyl orange dyes. It was also discovered that the composite enhanced the efficiency of dye degradation.

Various techniques are used to fabricate ternary oxide-based nanocomposites, including sol– gel, hydrothermal, co-precipitation, wet chemical, solvothermal, and successive ionic layer adsorption and reaction (SILAR) techniques [19–24]. Of the techniques mentioned above, the SILAR method is preferred for synthesizing nanocomposites because of its simplicity, efficiency, low growth temperature requirement, eco-friendliness, and cost-effectiveness [25,26].

The primary environmental concern facing all developing countries today is the explosion of organic contaminants in aquatic ecosystems, which is a result of continued technical advancements, industrialization, and rapid population expansion. A diverse range of toxic pollutants, predominantly in the form of dyes, are discharged from a multitude of industrial sectors, including textile manufacturing, printing, food processing, and paint manufacturing. The dyes, including methylene blue (MB), methyl orange (MO), p-nitroaniline (P-Nitro), rhodamine B (RhB), and cresol red (CR), with their complex organic structures, contribute to eutrophication pollution and pose a significant risk to aquatic ecosystems. Many methods, including sedimentation, adsorption, ion exchange, chemical processes, and photocatalytic reactions, have been used to remove these contaminants from wastewater. The utilization of semiconductor oxide photocatalysts for the photocatalytic degradation of organic pollutants in wastewater represents an efficient approach to the complete elimination of these stubborn contaminants. Furthermore, the photocatalytic process enjoys widespread adoption due to its generation of non-toxic byproducts, its utilization of solar energy within the visible spectrum, and its ease of operation [10,11,27–30].

At this time, environmentally friendly catalytic activities are gaining more interest, and the photocatalytic approach ensures a method for controlling the matter. Nanostructured semiconductor materials have been extensively used as photocatalysts owing to their distinctive structural, optical, electrical, and catalytic abilities. Hence, the photocatalytic performance of all synthesized films was investigated by degrading the MB dye under UV light.

In the decade, different nano-scale metal-oxide particles have been accomplished as hopefully photocatalysts for the degradation of organic pollutants and dyes and as a consequence of their wide optical bandgap and electronic structures, as well as their high abundance and chemical stability in aqueous solutions. The encouraging regulation of the electronic structure, light transmission or absorption characteristics, and charge transport properties of nanostructured metal-oxides has made its implementation as a photocatalyst feasible [31]. They have wide technological importance in electronics and environmental remediation due to their capability to generate charge. Although unary forms of metal-oxide particles have been frequently used for this purpose, research on ternary structures is still at an early stage. For this purpose, in this research, the three most widely known metal-oxides were preferred and their main physical characteristics, and photocatalytic efficacy were investigated.

To the best of our knowledge, there have been few studies on the production of ternary composites of ZnO, CuO, and CdO metal oxides as well as their physical properties. In this study, we fabricated single films of ZnO, CuO, and CdO as well as a ZnO–CuO– CdO multiple NC film using a cost-effective and simple SILAR method. The aim of this study was to investigate the physical and photocatalytic properties of the films. Advanced analysis methods, such as FESEM, XRD, UV– vis, FTIR, and TLM, were used to investigate the physical characteristics of the single films and NCs.

2. Experimental details

In this experiment, unary ZnO, CuO, CdO, and ternary ZnO-CuO-CdO metal oxide thin film materials were fabricated on soda lime glass substrates using the SILAR procedure. A.R. grade Cupric chloride dihydrate ($Cl_2CuH_4O_2$, ≥ 99.0%, Merck), Zinc(II) acetate dihydrate ($C_4H_{10}O_6Zn$, ≥ 99.0%, Merck), and Cadmium diacetate dehydrate ($C_4H_{10}CdO_6$, 98%, Merck) precursors were used without any modification. The glass substrates were cleaned using acetone (CH_3COCH_3, ≥ 99.5%, Sigma-Aldrich) and sulfuric acid solution (H_2SO_4, 98.0%, Sigma-Aldrich), rinsed with deionized water, and ultrasonically treated before the production of the films. To improve their adherence to the glass slides, they were thereafter allowed to air dry. 0.1 M concentrations of these salts were dissolved in 100 mL of deionized water to obtain a Zn^{2+}- Cu^{2+}-Cd^{2+}solution. These growth solutions were stirred for 10 min. to ensure that they were more transparent and homogeneous. The temperature of the growth baths and deionized water were adjusted to 85 °C and remained stable at this value during the experiment. One SILAR cycle includes two steps: immersion in a growth bath solution and then rinsing in deionized water. Soda-lime substrates were first immersed in prepared aqueous solutions and then in deionized water to suspend weakly bound ions from the substrate material. These operations were conducted for 15 s. The dipping and rinsing stages were recurrent 18 times to supply the requested thickness of unary and ternary thin film materials. This process was repeated separately for each metal. The manufactured unary and ternary thin film materials were annealed at 625 K for 2 h in air.

The surface morphology of the unary and ternary thin films was recorded using field emission scanning electron microscopy (FE-SEM) (JEOL SEM model JEM-5610 LV). In addition, elemental components and mapping were performed using an energy-dispersive X-ray spectrometer (EDX) connected to the FE-SEM equipment. The structural properties of the fabricated samples were investigated by using Cu Kα radiation source ($\lambda = 1.5406$ Å) in the range of $2\theta = 20°–80°$. The optical band gap properties were estimated using a UV–Vis. Spectrophotometer. The chemical bonding features of the samples were examined using Fourier transform-infrared (FT-IR) spectroscopy. The conductivity characteristics (I-V) of the unary and ternary thin films were determined via computer-controlled Agilent B2912A SMU at 300 K and in the dark. The transfer length method (TLM) was applied to establish the electrical resistance. Managing the SMU and data staging was conducted using VEE Pro-based SeCLaS software.[32]

The photocatalytic performance of unary and ternary materials on MB was surveyed by investigating a DIY photo reactor equipped with 385 nm UV led lamps driven by a 3 W constant current source at room temperature. The photocatalytic activity of the ternary nanostructured composite was examined using a methylene blue (MB) dye solution with stirring under a UV LED (3 W) positioned 10 cm above the reaction

mixture. For the photocatalytic process, 20 mg of ZnO-CuO-CdO composite powder was dissolved in 20 mL aqueous solutions of MB at specific pH and concentration (10 ppm). The samples were collected after starting from 5 min every 10 min at regular intervals to establish the MB degradation efficiency. Periodically, 3 mL of the suspensions were aggregated, centrifuged, and examined using a UV–vis. spectrometer. MB degradation was determined by using the change in the violence of the incorporated representative band absorption at 635 nm. To determine the concentration alteration of dye solutions, the UV–vis spectrum was recorded. The color of the dye (MB) solutions started to diminish with an increase in irradiation time. After 20 min, the MB dye solution took 120 min, confirming the degradation of the nanosized composites. The degradation efficiency (η) was calculated using the following relation [33,34]:

$$\eta = (C_0 - C_t/C_0)x100\% \quad (1)$$

where C_0 is the initial concentration and C_t is the concentration (mg/l) after irradiation at different time intervals.

Manufacturing nano-scale materials by using metal-oxides based structures to exterminate pollutants from waste water is the most famous field for research interests [35,36]. Noteworthy volumes (~10%) of synthetic dyes are preferred in industrial applications, and medical laboratories have a comprehensive influence on public health and the environment owing to their high toxicity. Various approaches have been employed to extirpate the organic contaminants. For this aim, the solar photocatalytic methodology is imagined to be an influential attempt to reduce the inverse environmental impact of hazardous water wastes and organic pollutants in aquatic ecosystems. This research has revealed that the ternary form of metal-oxide nanocomposites has a boosted sensing ability towards organic pollutants compared to unary-phase materials.

3. Results and discussion

Surface morphological examinations of the fabricated materials play a significant role in establishing the surface characteristics and nature of nanostructured materials. Hence, FESEM was used to characterize the shape, size distribution, and morphology of manufactured unary and ternary thin film nanostructures. Fig. 1. FESEM images of the unary ZnO, CuO, CdO, and ternary ZnO–CuO–CdO metal oxide thin film nanocomposites. It is clear that all of the films have smooth and homogeneous dense surface morphological features, crystallized structures, and the spherical and nanorod-like hybrid morphology of the as-synthesized ZnO–CuO–CdO nanocomposites. The implementation of three different metal oxides altered the morphology and kinetics of particle creation in nanostructured thin films. It is observable that the ternary metal– oxide structure has large accumulation, which is owing to the interaction between 3 different metals of oxides that convert the size, morphology, and kinetics of grown particles [37–39]. The changes in particle structures may be interrelated with the different electronegativity and atomic radius of the source elements, which influence the thermodynamically stable growth process and free surfaces of the crystal faces of ternary ZnO–CuO–CdO. A similar structure was also obtained from Munawar et al. [40] for the same ternary nanocomposite. The particle size and distribution of binary metal-oxide samples were transfigured with a ternary component and these outcomes have a good agreement with the XRD analysis.

The elemental composition analyses and surface mapping of the ZnO-CuO-CdO nanocomposite material revealed the elements' peaks in the spectra. The obtained EDX result clearly represented the presence of zinc, copper, and cadmium with percentages of 24.7%, 21.0%, and 35.9%, respectively, and oxygen at 18.4% (Fig. 2). As seen in the mapping, Zn is represented by red, Cu by navy blue, Cd by turquoise, and O by green. The absence of any other peaks related to impurities further evidenced the purity of the manufactured materials.

X-ray diffraction (XRD) was used to analyze the phase compositions and crystal structures of the produced films. The XRD diffraction peaks of the ZnO–CuO– CdO ternary nanocomposite structures and nanostructured unary ZnO, CuO, and CdO films are displayed in Fig. 3. The diffraction patterns of the films are in the wurtzite structure of hexagonal ZnO complying with JCPDS No 00–036–1451[41], in the polycrystalline structure with monoclinic phase of CuO complying with JCPDS No 01–072–0629 [42], and in the polycrystalline surface-centred cubic structure of CdO complying with JCPDS No 05–0640 [43]. Peaks related to ZnO are identified as lines (100; 2θ=31.75°), (002; 2θ=34.42°), (101; 2θ=36.26°), (102; 2θ=47.54°), (110; 2θ=57.00°), (103; 2θ=62.87°), (112; 2θ=67.95°), and (201; 2θ=69.07°) [44]. CuO can be represented by various lines, including (110; 2θ=32.45°), ($\bar{1}$11; 2θ=35.53°), (111; 2θ=38.65°), ($\bar{2}$02; 2θ=48.87°), (020; 2θ=53.40°), (202; 2θ=58.31°), ($\bar{1}$13; 2θ=61.56°), ($\bar{3}$11; 2θ=66.25°), and (220; 2θ=67.99°) [45]. CdO corresponds to planes (111; 2θ=32.92°), (200; 2θ=38.21°), (220; 2θ=55.19°), and (311; 2θ=65.81°) [46]. The XRD pattern did not reveal any additional diffraction lines related to the hydroxides and impurity phases, except for the diffraction images of ZnO, CuO, CdO, and the ZnO–CuO– CdO composite. The XRD spectra of the synthesized films show sharp and dominant diffraction lines, indicating high crystallinity of both the unary ZnO, CuO, and CdO films, as well as the ZnO–CuO– CdO ternary composite film.

The average crystal size (*D*) values were calculated using Scherrer's relation [47], considering only the dominant peaks in the XRD picture.

$$D = \frac{0.94\lambda}{\beta\cos\theta} \quad (2)$$

In Scherrer's equation, λ, β, and θ correspond to the wavelength, full width at half height, and Bragg's angle of the X-ray, respectively. The *D* values of unary ZnO, CuO, CdO, and ZnO–CuO– CdO ternary films were found to be 18.71, 12.86, 15.88, and 21.96 nm, respectively (Table 1). The *D* value of the ZnO–CuO– CdO ternary nanocomposite film is attributed to the varying ionic radii of ZnO (Zn^{2+}: 0.60 Å), CuO (Cu^{2+}: 0.57 Å), and CdO (Cd^{2+}: 0.78 Å) in the respective single MOs. The situation in D may be attributed to the combination of ZnO, CuO, and CdO MO materials in a single lattice structure in the synthesized films [40,48,49]. These structural alterations also have a good compromise with the particle thickness observations from the FESEM images.

The Fourier transform infrared (FT-IR) method was employed to validate the existence of significant functional groups present in the samples. The modes of FT-IR are influenced by particle size, shape, and accumulation state. The recorded FT-IR spectra of the ZnO, CuO, CdO, and ternary samples are displayed in Fig. 4. in order to verify their structures. As illustrated in Fig. 4, the prepared samples' FT-IR spectra in the wavenumber range of 500–4000 cm^{-1} revealed the existence of numerous vibrational modes.

Metal-oxide materials typically show absorption bands in the fingerprint area (below 1000 cm^{-1}) due to interatomic vibrations [50]. The vibration mode for pure CdO was observed at 548 cm^{-1} [34]. The peaks observed at 878, 751, and 674 cm^{-1} can be attributed to the stretching modes of metal–oxygen (M–O) (M = Zn, Cu, Cd). FT-IR spectra confirmed the successful formation of nanocomposites via the presence of metal– oxygen bonds. These consequences affirm the acquired structure of the nano-scale ternary composite and are well supported by the XRD results.

The peaks in the functional group regime are the result of residual precursors, organic contaminants, and CO_2 from the air interacting with the metallic cations. The intense peak at 2350 cm^{-1} was attributed to the stretching vibrations of CO_2 [51]. The weak peak intensities of absorption indicate the existence of water molecules within the thin films. Weak peaks at 3740 and 3678 cm^{-1} were identified as the stretching vibration of the OH group [52]. Additional bands around 3000–2900, and 1600–1000 cm^{-1} that were attributed to additional chemical bonding, may have resulted from the deformation and bending

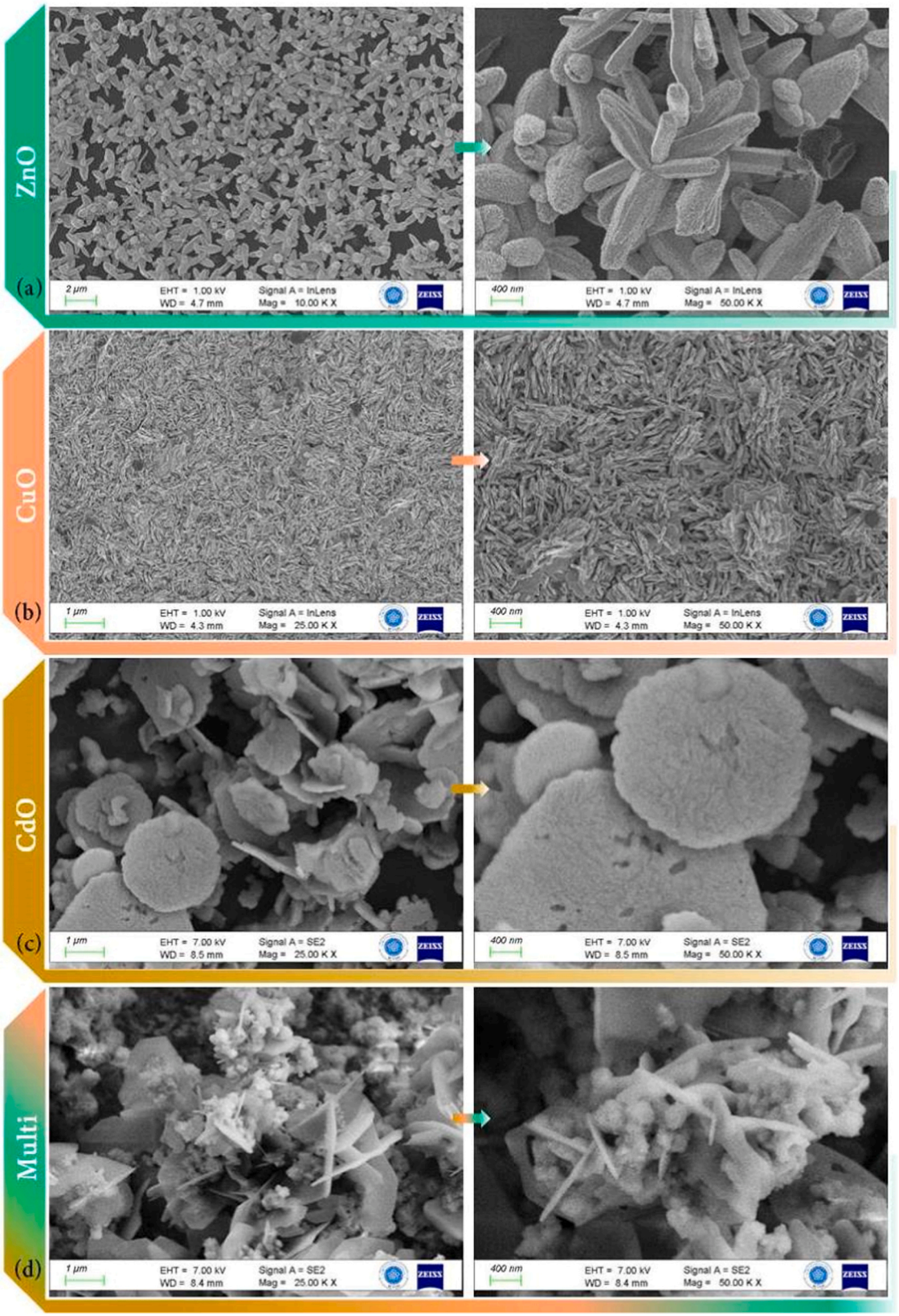

Fig. 1. FESEM images of unary ZnO, CuO, CdO, and ternary ZnO-CuO-CdO nanocomposite thin film materials. It is clear that all of the films have smooth and homogeneous dense surface morphological features, crystallized structures, and the spherical and nanorod-like hybrid morphology of the as-synthesized ZnO–CuO–CdO nanocomposites.

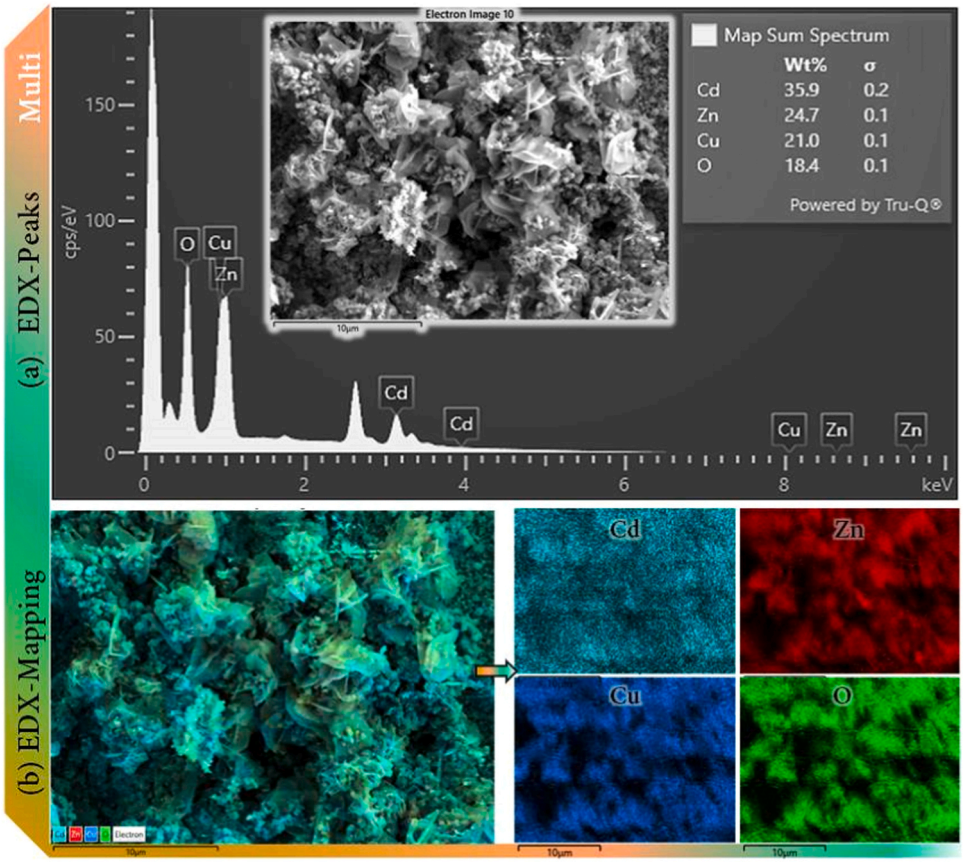

Fig. 2. Energy dispersive X-ray spectroscopy elemental maps of Zn, Cd, Cu and O in ternary ZnO-CuO-CdO nanocomposite thin film materials. The obtained EDX result clearly represented the presence of zinc, copper, and cadmium with percentages of 24.7%, 21.0%, and 35.9%, respectively, and oxygen at 18.4%.

vibrations of chemisorbed or physically absorbed CO and CH_2-CH_3 molecules [53]. The vibration modes resulting from different chemical bonds were identified: 1577 and 1063 cm^{-1} for CO stretching vibrations caused by air and 2979, 2905, 1400 and 1245 cm^{-1} for CH_2-CH_3 vibrations.

The optical phonon frequency (ν_0) may be determined from FT-IR spectra by analyzing the observed bands associated with the vibrations of ZnO, CdO, and CuO bonds. ν_0 is the optical phonon frequency (Hz), ν is the wave number (cm^{-1}) and λ is the wavelength (cm). Calculations for ν_0 and Debye temperature θ_D were performed on the basis of the observed vibration of CuO, ZnO, and CdO bonds using the equations: $c = \lambda\nu_0 = \nu_0/\nu$ and $h\nu_0 = k_B\theta_D$, where h and k_B are the Planck's constant and Boltzmann constant [34,54].

$$\nu = \frac{1}{2\pi c}\left(\frac{k}{\mu}\right)^{1/2} \tag{3}$$

Eq. 3 can be used to calculate the force constants of CuO, ZnO, and CdO. where k is the force constant, c is the speed of light (3.00×10^{10} cm/s) and μ is an effective mass of ZnO, CdO, and CuO given by $\mu = \frac{m_1 X m_2}{m_1+m_2}$, where m_1 and m_2 are the atomic weights of the bounded atoms [54,55]. Table 2 contains the values of the vibrational parameters that have been computed.

UV–vis spectra of unary ZnO, CuO, CdO, and ternary ZnO–CuO–CdO composites are presented in Fig. 5. The absorption intensities of ZnO, CdO, and CuO are higher than those of ZnO–CuO–CdO nanostructures. The rough surface of the composites would allow more light for absorption than the smooth surface of bare CuO, ZnO, and CdO. These results imply that the photocatalytic performance of ternary ZnO–CuO–CdO is higher than that of unary metal oxides. The characterization results imply that the ZnO–CuO–CdO nanocomposite may be a good candidate material for optoelectronic and photocatalytic applications.

The utilization of nanostructured metal-oxide materials for photocatalytic degradation of different dyes is an economically friendly procedure; hence, there is no requirement to supplement any expensive chemical materials, like capping or reducing agents. For the implementation of enhanced wastewater treatment procedures on an industrial scale, it is not avoidable that they should be environmentally and economically sustainable. The economic cost of fabricated materials for photocatalytic degradation largely depends on the type of equipment and facilities and on market demand. In this experiment, preferred metal sources like Zn, Cd, and Cu are abundant sources in nature that are easily available [56].

Methylene blue (MB) as a heterocyclic dye has been comprehensively used in industrial implementations, having diverse impacts on ecosystems and public health owing to their high toxicity. In this research, the utilization wavelength in the visible light region (390 nm) for photocatalytic degradation of pollutants is found to be the best option at the industrial scale; hence, solar light is a safe, clean, and most economical light source.

Degradation mechanism of MB under UV light irradiation occurs in 4 steps [33,34,57];

1. photo excitation of metal oxides and creation of electron (e^-) / hole (h^+) pairs with UV photons:

$$\text{CdO-CuO-ZnO} + h\nu \rightarrow \text{CdO-CuO-ZnO} + (e^- + h^+) \tag{4}$$

2. oxygen absorption of metal oxides:

$$\text{CdO-CuO-ZnO}\ (e^-) + O_2 \rightarrow \text{CdO-CuO-ZnO} + \bullet O_2^- \tag{5}$$

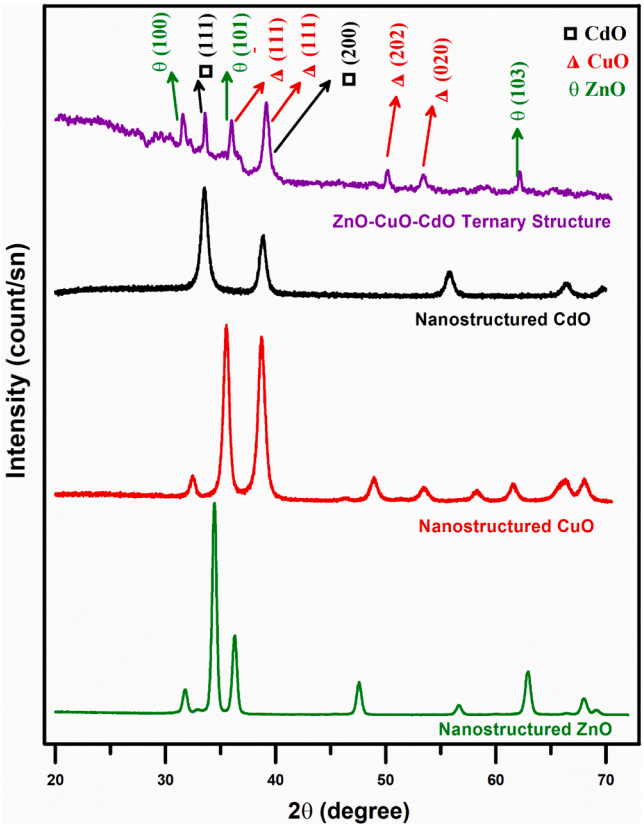

Fig. 3. X-ray diffraction patterns of unary ZnO, CuO, CdO, and ternary ZnO-CuO-CdO nanocomposite thin film materials. It shows sharp and dominant diffraction lines, indicating the high crystallinity of both the unary and ternary composite films.

Table 1
Crystallite size and optical bandgap values of ZnO, CuO, CdO and ZnO-CuO-CdO films.

Sample Name	Crystallite Size (nm)	Optical Bandgap (eV)
ZnO	18.71	3.20
CuO	12.86	1.47
CdO	15.88	2.21
ZnO-CuO-CdO	21.96	2.51

3. ionization of water molecules:

$$H_2O \rightarrow H^+ + OH^- \quad (6a)$$

$$\bullet O_2^- + 2H^+ + e^- \rightarrow H_2O_2 \rightarrow 2\ \bullet OH \quad (6b)$$

4. protonation of excited oxides:

$$\bullet OH + MB \rightarrow \text{Degraded products} \quad (7a)$$

$$\bullet O_2^- + MB \rightarrow \text{Degraded products} \quad (7b)$$

The band gap energy values of ZnO, CuO, CdO, and ternary ZnO–CuO–CdO were relatively low, and UV irradiation excites an electron from the valence band of these oxides to the conduction band, leaving holes in the background (in the valence band) (step 1.). These excited electrons tend to create superoxide radical anion (step 2.) and hydroxide radicals (step 3), which both are highly reactive, and finally, they oxidize the MB molecules (step 4).

The ZnO–CuO–CdO nanocomposite attacks the carboxylic acid formed by the degradation of aromatic rings because of the photocatalytic effect of MB and the acetate ions in the solution. Because the solubility product of copper is smaller than that of cadmium and zinc, a copper acetate compound is formed. This could correspond to the opening of aromatic rings with the transient formation of carboxylic acids. This compound, which has a water solubility of 43.7 g/L, can easily form like zinc acetate (30 g/100 g H_2O) and cadmium acetate and gives a blue color to the solution (as given in Eq. 8). As a result, there is a slight increase in the absorbance peak in the UV spectrum. A schematic representation of the photocatalytic degradation measurement setup is described in Fig. 6.

$$C_4H_{10}O_6Zn + Cl_2CuH_4O_2 + C_4H_{10}CdO_6 \rightarrow Cu(CH_3COO)_2 + Zn^{2+} + Cd^{2+} + Cl^- + C_4H_{10}O_6^- \quad (8)$$

All the results indicate that degradation kinetics were in a second-order process until 40 min, followed by a first-order process [58] (Fig. 7). When copper, zinc, and cadmium oxides are applied separately to MB adsorption, removal occurs at a linearly increasing rate and reaches a constant value after a while 20 min (Fig. 8). Similar increased photocatalytic performance was recorded for CuO–ZnO compared to bare CuO and ZnO. As in the study by Harish et al. for ZnO–CuO–CdO, it was observed that the photocatalytic adsorption, which began with a higher acceleration, started to decrease after a while and then remained constant again [33]. The ZnO–CuO–CdO composite reached a 70% removal value in 20 min, then reached a 60% removal value in 40 min, a 50% removal value in 60 min, and remained constant thereafter (Fig. 8). It has been observed that photocatalytic degradation occurs in an increasing linear change for all CuO, ZnO, CdO, CuO/ZnO, and ZnO–CuO– CdO composites between 0 and 20 min (Fig. 8). All these results indicate that degradation kinetics were in a second-order process until 40 min, followed by a first-order process [58]. Different researchers have affirmed the important effects of the crystallite size on the photocatalytic performance. It is usually considered admirable for the crystallite size of a photocatalyst to be nano-scale; i.e., the specific surface area should be extensive. Obtained nano-scale particle size leads to easy transport of photogenerated electrons (e^-) and holes (h^+) [59–61].

The degradation efficiency of ternary ZnO-CuO-CdO composite reaches a maximum value about 20 minutes and the kinetic degradation rate (ln (C_0/C_t)) value was determined as 0.46. This result is in good agreement with the literature (Table 3).

Metal-oxide based nanostructured photocatalysis offers a permanent adjustment for cleaning up contaminated environments. When appropriate metal-oxide materials are exposed to artificial light or sunlight, they generate electron-hole pairs, thus decomposing contaminants from contaminated environments and boosting air and water quality [65,66]. These features makes them an important and suitable candidate for applications ranging from drinking water treatment to wastewater purification in both domestic and industrial areas.

The absorbance in the UV–vis. spectra is commanded by the bandgap energy (E_g) of a metal-oxide semiconductor material, which is correlated with the optical absorption coefficient (α) and the incident photon energy ($h\upsilon$) by the following relation:

$$(\alpha h\upsilon) = C\left(h\upsilon - E_g\right)^{1/2} \quad (9)$$

where C is an energy-independent constant and E_g is the optical bandgap energy value [67]. Fig. 9 shows the plots of $(\alpha h\upsilon)^2$ versus $h\upsilon$ of unary ZnO, CuO, CdO, and ternary ZnO–CuO– CdO nanostructured composite thin films. The estimated E_g values were found to be 3.20, 1.47, 2.21, and 2.51 eV for the ZnO, CuO, CdO, and ternary ZnO–CuO–CdO films, respectively (Table 1). Every component of the ternary ZnO–CuO– CdO nanocomposite thin film presents various energy gaps, such as ZnO has ~3.37 eV [68], CdO has ~2.3 eV [69], and CuO having a smaller energy gap of 1.5 eV [25]. This segregation in the optical energy gap values of

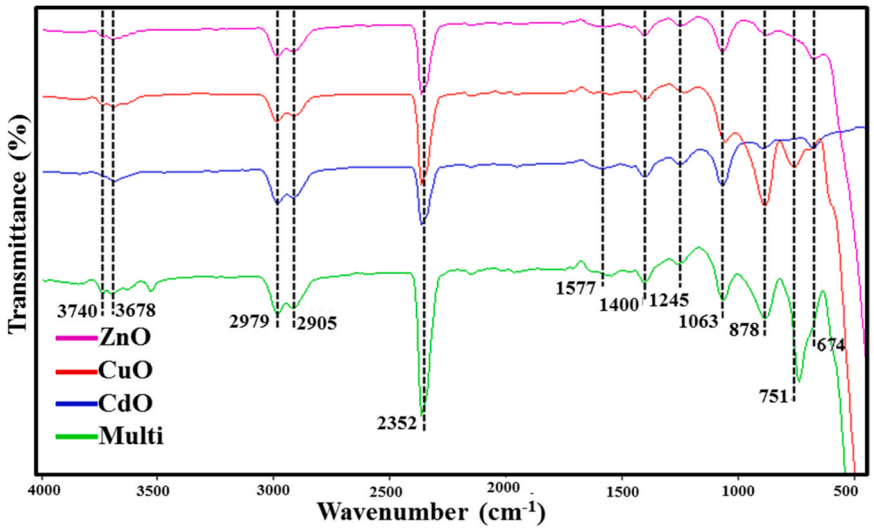

Fig. 4. FT-IR spectra of unary ZnO, CuO, CdO, and ternary ZnO-CuO-CdO nanocomposite thin film materials. The prepared samples' FT-IR spectra in the wavenumber range of 500–4000 cm^{-1} revealed the existence of numerous vibrational modes.

Table 2
FT-IR bands, force constant, effective mass, optical phonon frequency, and Debye temperature rates for the unary ZnO, CdO, and CuO samples.

Unary Oxides	Wavenumber (cm^{-1})	Effective mass (10^{-26} kg)	Force constant, k (N/cm)	Optical phonon frequency, ν_0 (Hz) 10^{13}	Bending Debye temperature θ_D (K)
ZnO	878	2.1343	5.8460	2.634	1260
CuO	751	2.1224	4.2533	2.253	1080
CdO	674	2.3256	3.7538	2.022	970

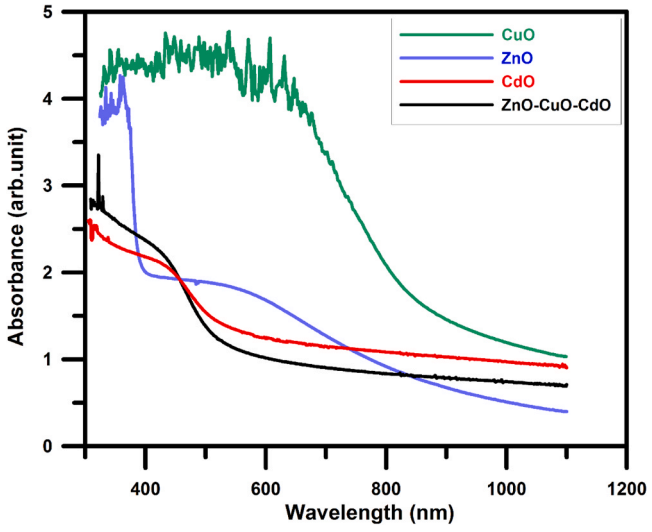

Fig. 5. UV–vis absorbance for unary ZnO, CuO, CdO and ternary ZnO-CuO-CdO nanocomposite thin film materials. The absorption intensities of ZnO, and CuO are higher than those of ZnO–CuO–CdO nanostructures. The rough surface of the composites would allow different light for absorption than the smooth surface of bare CuO, ZnO, and CdO.

unary materials affects the entire energy gap manner of the nanostructured ternary metal oxides. The singular features and electronic structures of each metal oxide create the integrated energy gap of the ternary composite thin film materials. Accordingly, by mixing the three

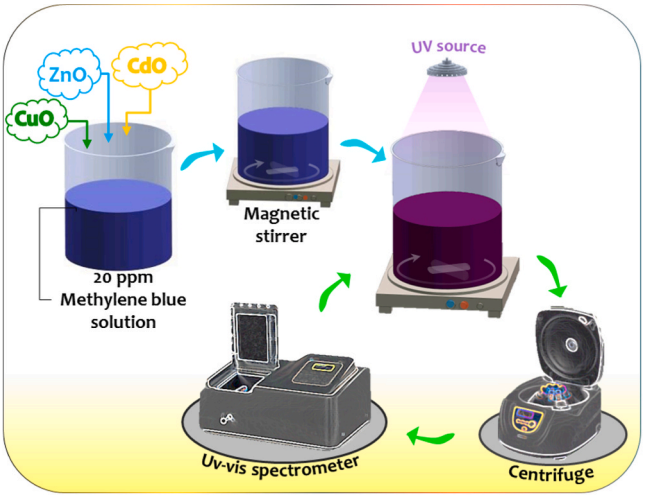

Fig. 6. Schematic representation of photocatalytic degradation measurement setup.

different metal-oxide materials, the bandgap energy can be engineered to make the nanostructured ternary composite material suitable for several applications, such as photocatalysis, optoelectronics, and electronic devices.

The electrical conduction mechanism of thin films is different from that of bulk materials. In bulk materials, the current conduction mechanisms depend on the properties of the material, and the properties of the surface are usually not taken into account, whereas in thin films, the conductivity is tightly coupled to both the properties of the bulk material and the surface properties of the thin films. However, many parameters, such as the thickness of the films, annealing temperature, the size of the crystals forming the film, the conductivity behavior at domain boundaries, the presence of dopant atoms and defects that form the basis of current conduction, especially in metal oxides, and their densities, affect the conductivity mechanism [70–74]. Therefore, when producing devices based on the electrical properties of materials, a method such as the transfer length method (TLM) (Fig. 10), which can account for both the properties of the contact and current conduction in thin films, such as current crowding, should be considered [75].

In this method, contact distances and series resistance (R_T) parameters, calculated from current– voltage (I-V) measurements between

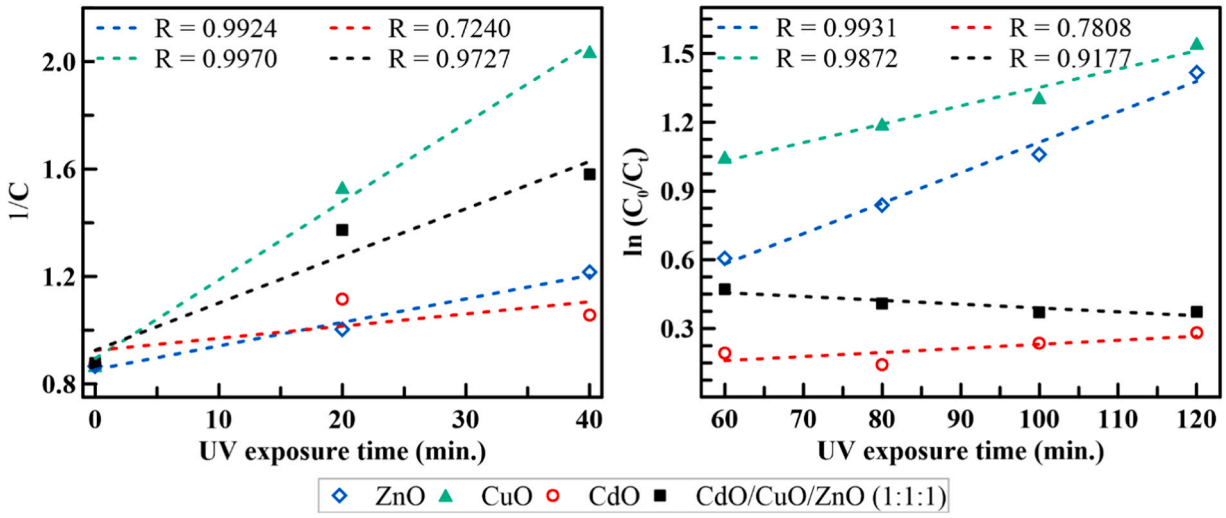

Fig. 7. Degradation kinetics of MB in unary and ternary composite samples. All the results indicate that degradation kinetics were in a second-order process until 40 min.

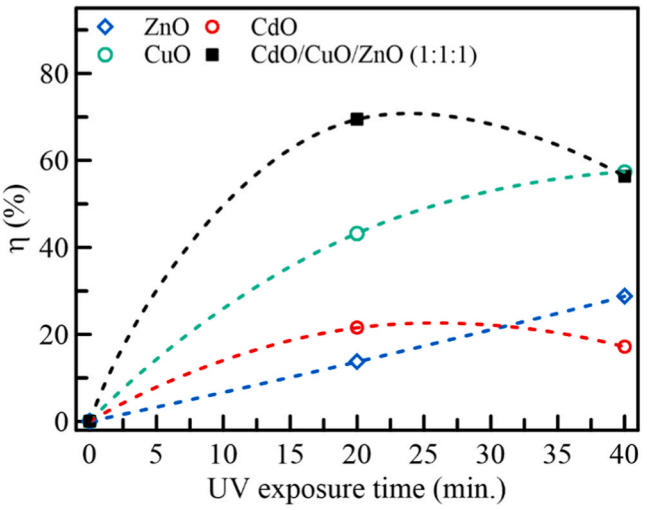

Fig. 8. Removal percentage of MB by unary and ternary composite samples. When copper, zinc, and cadmium oxides are applied separately to MB adsorption, removal occurs at a linearly increasing rate and reaches a constant value after a while 20 min.

Table 3
Comparison of photocatalytic performance of ternary CuO-CdO-ZnO nanomaterials on the degradation of MB dye pollutants.

Photocatalysts	ln (C_0/C_t)*	Refs.
ZnO-CuO	0.20	[62]
ZnO-CuO (15% wt.)	1.15	[63]
CdO-ZnO	0.45	[64]
ZnO-NiO-CuO (1:1:1)	0.45	[50]
NiO-Fe_2O_3-CdO	0.40	[4]
CuO-CdO-ZnO	0.46	Present work

* Some values here were obtained pointwise from the relevant graphs.

these contacts, can be plotted. Using the data from these graphs and the relations given below, the effective transfer length (L_T), which is an important parameter for load transport, and the specific contact resistance (ρ_c), which is important for device manufacturing, can be calculated. In such a case, the slope and intercept of *the d* vs. R_T plots give the total contact resistance (R_C) and the L_T with the following equations [75,76]:

$$R_c = \frac{R_{Sk}L_T}{w}\coth(d/L_T) \tag{10}$$

and

$$L_T = \sqrt{\frac{\rho_c}{R_{Sk}}} \tag{11}$$

where w, d and R_{Sk} is the width of the contact, length of the contact, and modified sheet resistance under the contact, respectively. Current–voltage measurement results of unary ZnO, CuO, CdO, and ternary ZnO–CuO– CdO metal oxide thin film nanocomposites are given in Fig. 11 a–d. All metal oxide thin films showed ohmic behavior, and resistivity values depended on their unique nature.

The DC resistivity values decreased with pad distance. The calculated R_T values are given in Fig. 12. (a-c) for each thin film nanocomposite. CdO was the most conductive film, and the resistivity values of CuO were higher than those of other films. We expected that the resistivity values of ternary ZnO–CuO–CdO thin film nanocomposites would differ between CdO and CuO. Also, calculated lowest and highest L_T and ρ_c values belongs to CdO and ZnO thin films, respectively (Fig. 12 (d-e)).

Specific contact resistivity values were 347.33 Ωcm^2, 213.33 kΩcm^2, 780.83 kΩcm^2 and 1.97 kΩcm^2 for CdO, CuO, ZnO, and ternary ZnO–CuO–CdO thin films, respectively. The conductivity of metal oxides mainly depends on their density of oxygen vacancies [72,73], and the influence of some morphological parameters (e.g. film quality, particle distribution, and size surface roughness, etc.) should be considered [37,48]. CdO films grown by the SILAR method have very low sheet resistances (about 10^{-3} Ωcm for annealed samples) because of the high carrier concentration density [71,77]. The effects of this high carrier concentration are also clearly observed in the ternary film for values of ρ_c and L_T. CuO and ZnO thin films grown by the SILAR method have relatively higher specific contact resistivity values due to the lower oxygen vacancy density.

4. Conclusions

As a conclusion, bare unary ZnO, CuO, CdO, and ternary ZnO-CuO-CdO oxide nanostructured composite thin films were fabricated by the low-cost SILAR method. The XRD pattern supported the creation of nanocomposites with ZnO (hexagonal), CuO (monoclinic), and CdO (cubic). The alteration in crystallite size was recorded because of the interaction of three different metal-oxides. It was apparent that all of the

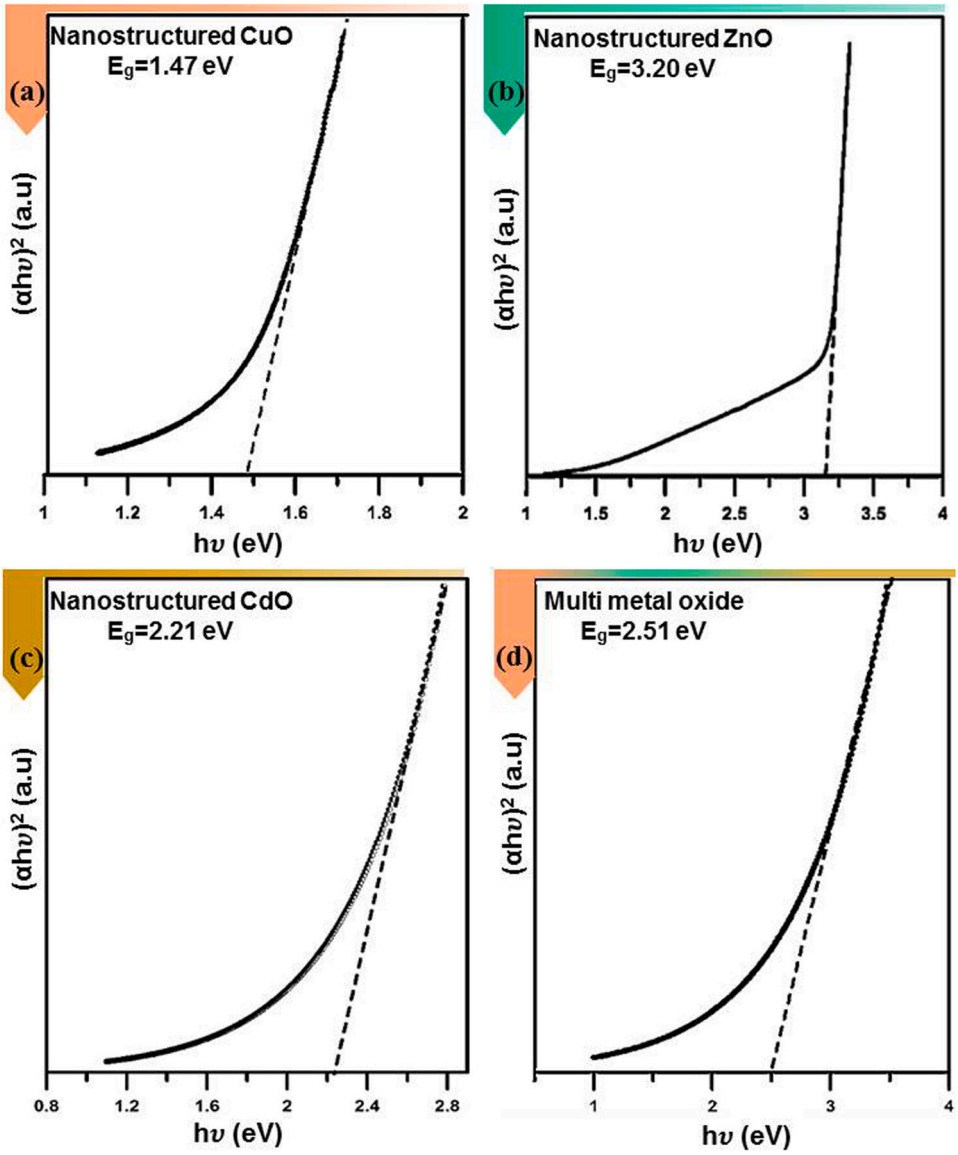

Fig. 9. Optical band gap energy values of unary ZnO, CuO, CdO and ternary ZnO-CuO-CdO nanocomposite thin film materials. The estimated *Eg* values were found to be 3.20, 1.47, 2.21, and 2.51 eV for the ZnO, CuO, CdO, and ternary ZnO–CuO–CdO films, respectively. The singular features and electronic structures of each metal oxide create the integrated energy gap of the ternary composite thin film materials.

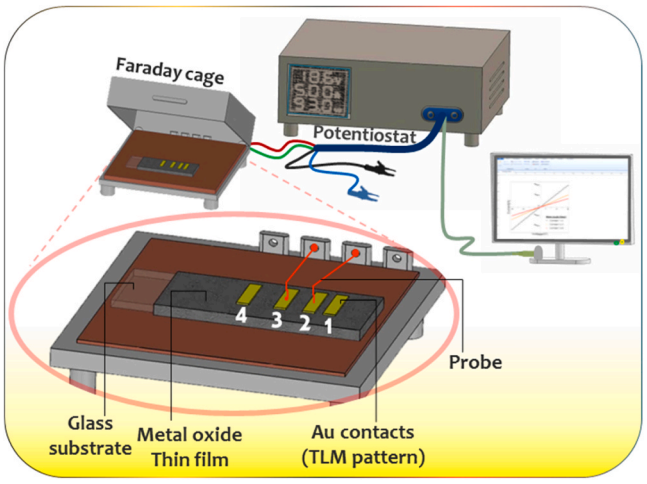

Fig. 10. Experimental setup of electrical measurement system by TLM method.

films have smooth and homogeneous dense surface morphological features, crystallized structures, and the spherical and nanorod-like hybrid morphology of the as-synthesized ZnO–CuO– CdO nanocomposites. The XRD, EDX, and FTIR, confirmed the formation of the ZnO-CuO-CdO nanocomposite structure. The photocatalytic degradation investigations exhibited boosted efficacy of the ZnO-CuO-CdO ternary composite for the degradation of methylene blue dye (70% in 20 min), which is demonstrated to be a propitious sunlight-driven photocatalyst. Additionally, the electrical behavior and photocatalytic performance of fabricated unary and ternary samples presented more effective and efficient results. The optical absorption properties, hence optical bandgap energy (E_g), and electrical conductivity were found to be strongly affected by the composition of nanostructured binary metal-oxides. The optical bandgap value was 2.51 eV calculated for ternary ZnO-CuO-CdO using UV–vis spectra. This obtained optical bandgap energy, which made the fabricated ternary nanocomposite an excellent photocatalyst under sunlight. Obtained photocatalytic outcomes introduce an innovative sunlight driven photo-catalyst for the degradation of MB as a heterocyclic dye. Accordingly, by mixing the three different

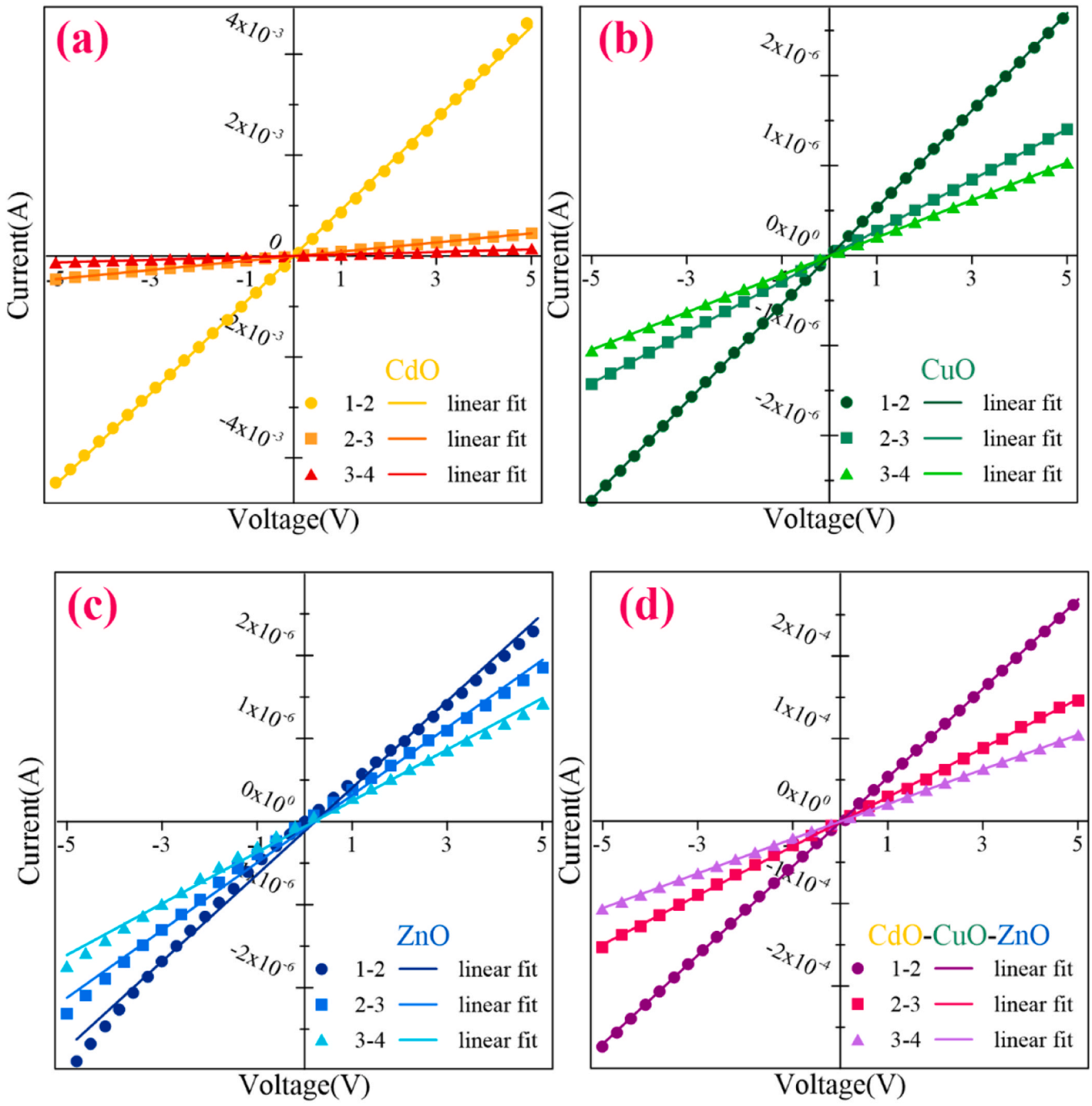

Fig. 11. I-V characteristics of unary CdO (a), CuO (b), ZnO (c) and ternary ZnO-CuO-CdO (d) metal oxide thin film nanocomposites. All synthesized metal oxide thin films showed ohmic behavior, and resistivity values depended on their unique nature.

metal-oxide materials, the bandgap energy can be engineered to make the nanostructured ternary composite material suitable for several implementations, such as photocatalysis, optoelectronics, and electronic devices. In this study, some descriptive thin film properties of each metal oxide forming the ternary composite film, as well as the properties of the ternary film and its synergetic effect, were revealed. Future research could be focused on sensing ability and investigating the role of thin film properties of each component in the ternary composite. In addition, different possible solutions can be tried to use the synthesized composite films in a large-scale process. Also, testing different dyes may be the subject of future research initiatives.

CRediT authorship contribution statement

Osman Kahveci: Writing – review & editing, Writing – original draft, Methodology, Data curation, Conceptualization. **Ebru Karakaş Sarıkaya:** Writing – original draft, Methodology, Data curation. **Abdullah Akkaya:** Writing – review & editing, Writing – original draft, Resources, Data curation, Conceptualization. **Rasit Aydin:** Writing – review & editing, Writing – original draft, Methodology, Investigation. **Murat ÇANLI:** Methodology, Formal analysis, Data curation. **Enise Ayyıldız:** Methodology, Formal analysis. **Bünyamin Şahin:** Writing – review & editing, Writing – original draft, Supervision, Methodology, Data curation.

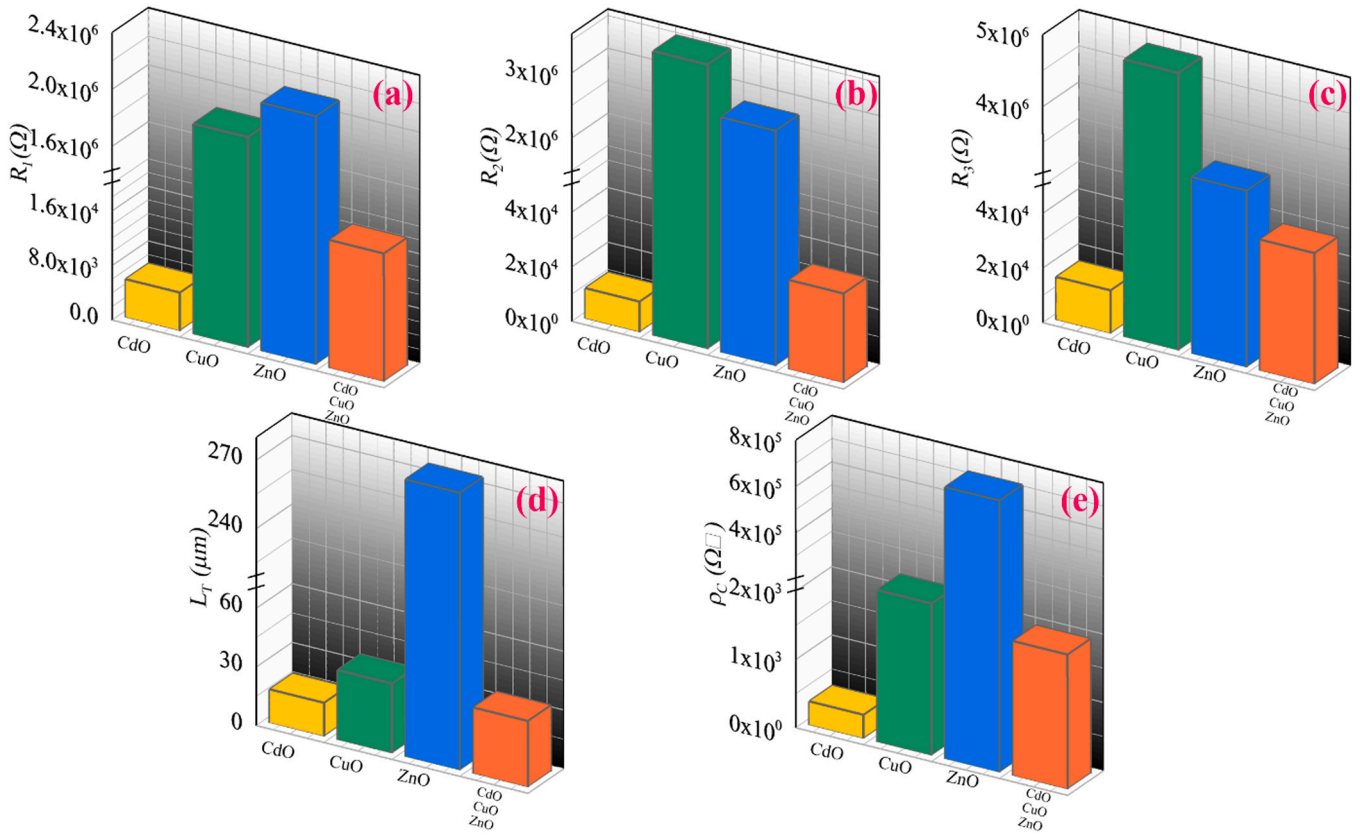

Fig. 12. Calculated R_1, R_2 and R_3 values between the contacts (a-c), L_T (d) and ρ_c (e) values of unary CdO, CuO, ZnO and ternary ZnO-CuO-CdO metal oxide thin film nanocomposites. Specific contact resistivity values are 347.33 Ωcm^2, 213.33 $k\Omega cm^2$, 780.83 $k\Omega cm^2$ and 1.97 $k\Omega cm^2$ for CdO, CuO, ZnO, and ternary ZnO–CuO– CdO thin films, respectively.

Declaration of Competing Interest

The authors declare that they have no known competing financial interests or personal relationships that could have appeared to influence the work reported in this paper.

Data availability

No data was used for the research described in the article.

References

[1] P. Kannan, G. Maduraiveeran, Metal oxides nanomaterials and nanocomposite-based electrochemical sensors for healthcare applications, Biosensors (2023).

[2] Y.F. Mustafa, Modern developments in the application and function of metal/metal oxide nanocomposite–based antibacterial agents, BioNanoScience 13 (2023) 840–852.

[3] M.H. Mohsin, K.S. Khashan, G.M. Sulaiman, H.A. Mohammed, K.A. Qureshi, A. Aspatwar, A novel facile synthesis of metal nitride@metal oxide (BN/Gd2O3) nanocomposite and their antibacterial and anticancer activities, Sci. Rep. -Uk 13 (2023) 22749.

[4] F. Mukhtar, T. Munawar, M.S. Nadeem, M. Hasan, F. Hussain, M.A. Nawaz, F. Iqbal, Multi metal oxide NiO-Fe_2O_3-CdO nanocomposite-synthesis, photocatalytic and antibacterial properties, Appl. Phys. A 126 (2020) 588.

[5] K. Kannan, D. Radhika, D. Gnanasangeetha, S.K. Lakkaboyana, K.K. Sadasivuni, K. Gurushankar, M.M. Hanafiah, Photocatalytic and antimicrobial properties of microwave synthesized mixed metal oxide nanocomposite, Inorg. Chem. Commun. 125 (2021) 108429.

[6] J. Khan, S. Bibi, I. Naseem, S. Ahmed, M. Hafeez, K. Ahmed, F. Altaf, D. Dastan, A. Syed, M.S. Jabir, M.K.A. Mohammed, L. Tao, Ternary metal (Cu–Ni–Zn) oxide nanocomposite via an environmentally friendly route, ACS Omega 8 (2023) 21032–21041.

[7] T. Munawar, S. Yasmeen, M. Hasan, K. Mahmood, A. Hussain, A. Ali, M.I. Arshad, F. Iqbal, Novel tri-phase heterostructured ZnO–Yb_2O_3–Pr_2O_3 nanocomposite; structural, optical, photocatalytic and antibacterial studies, Ceram. Int 46 (2020) 11101–11114.

[8] M.A. Rahman, S.M.N. Mamun, A.K.M.A. Hossain, C. Ton-That, ZnO nanorods on Li-doped ZnO thin films for efficient p–n homojunction light-emitting diodes, ACS Appl. Nano Mater. 6 (2023) 15757–15763.

[9] S. Mrabet, N. Ihzaz, M.N. Bessadok, C. Vázquez-Vázquez, M. Alshammari, L. El Mir, Microstructural, raman, and magnetic investigations on Ca-doped ZnO nanoparticles, J. Inorg. Organomet. Polym. Mater. (2023).

[10] X. Yu, T. Ai, K. Wang, Application of nanogenerators in acoustics based on artificial intelligence and machine learning, Apl. Mater. 12 (2024).

[11] X. Yu, Y. Shang, L. Zheng, K. Wang, Application of nanogenerators in the field of acoustics, ACS Appl. Electron. Mater. 5 (2023) 5240–5248.

[12] B. Liu, L. Tian, X. Zheng, Z. Xing, MnO_2 Films deposited on CuO nanomaterials as electrode materials for supercapacitors, J. Alloy Compd. 911 (2022) 165003.

[13] R. Javed, M. Ahmed, Iu Haq, S. Nisa, M. Zia, PVP and PEG doped CuO nanoparticles are more biologically active: antibacterial, antioxidant, antidiabetic and cytotoxic perspective, Mater. Sci. Eng.: C. 79 (2017) 108–115.

[14] M.H. Kabir, A. Bhattacharjee, M.M. Islam, M.S. Rahman, M.S. Rahman, M.K. R. Khan, Effect of Sr doping on structural, morphological, optical and electrical properties of spray pyrolized CdO thin films, J. Mater. Sci.: Mater. Electron. 32 (2021) 3834–3842.

[15] M. Anitha, N. Anitha, K. Saravanakumar, I. Kulandaisamy, L. Amalraj, Effect of Zn doping on structural, morphological, optical and electrical properties of nebulized spray-deposited CdO thin films, Appl. Phys. A 124 (2018) 561.

[16] A. Sankaran, K. Kumaraguru, The novel two step synthesis of CuO/ZnO and CuO/CdO nanocatalysts for enhancement of catalytic activity, J. Mol. Struct. 1221 (2020) 128772.

[17] K. Mubeen, A. Irshad, A. Safeen, U. Aziz, K. Safeen, T. Ghani, K. Khan, Z. Ali, I. ul Haq, A. Shah, Band structure tuning of ZnO/CuO composites for enhanced photocatalytic activity, J. Saudi Chem. Soc. 27 (2023) 101639.

[18] K. Sirohi, S. Kumar, V. Singh, N. Chauhan, A. Vohra, Facile synthesis of CdO–ZnO nanocomposites for photocatalytic application in visible light, Arab J. Sci. Eng. 49 (2024) 273–284.

[19] A.O. Juma, E.A.A. Arbab, C.M. Muiva, L.M. Lepodise, G.T. Mola, Synthesis and characterization of CuO-NiO-ZnO mixed metal oxide nanocomposite, J. Alloy Compd. 723 (2017) 866–872.

[20] A. Aslani, M.R. Arefi, A. Babapoor, A. Amiri, K. Beyki-Shuraki, Solvothermal synthesis, characterization and optical properties of ZnO, ZnO–MgO and ZnO–NiO, mixed oxide nanoparticles, Appl. Surf. Sci. 257 (2011) 4885–4889.

[21] P. Wang, J. Pan, J. Mei, Q. Yu, P. Wang, Z. Chen, J. Wang, C. Song, Y. Zheng, C. Li, Photovoltaic conversion enhancement of a transparent NiO/CdO/ZnO pn junction device with a CdO transition layer, J. Alloy Compd. 862 (2021) 158430.

[22] S. Saedy, M. Haghighi, M. Amirkhosrow, Hydrothermal synthesis and physicochemical characterization of CuO/ZnO/Al_2O_3 nanopowder. Part I: effect of crystallization time, Particuology 10 (2012) 729–736.

[23] M.M. Alam, A.M. Asiri, M.M. Rahman, M.A. Islam, Fabrication of sensitive D-fructose sensor based on facile ternary mixed ZnO/CdO/SnO_2 nanocomposites by electrochemical approach, Surf. Interfaces 19 (2020) 100540.

[24] J.-H. Lee, S. Heo, J.-I. Youn, Y.-J. Kim, I.-K. Kim, K.-W. Jang, H.-J. Oh, Photocatalytic Characteristics of PbS/ZnO/TiO_2 nanotube composite, Korean, J. Mater. Res. 27 (2017) 569–575.

[25] A. Akkaya, O. Kahveci, R. Aydın, B. Şahin, Amplifying main physical characteristics of CuO films using ascorbic acid as the reducer and stabilizer agent, Appl. Phys. A 127 (2021) 911.

[26] H. Latif, S. Ashraf, M. Shahid Rafique, A. Imtiaz, A. Sattar, S. Zaheer, S. Ammara Shabbir, A. Usman, A novel, PbS quantum dot-Sensitized solar cell structure with TiO_2-fMWCNTS nano-composite filled meso-porous anatase TiO_2 photoanode, Sol. Energy 204 (2020) 617–623.

[27] S. Batool, M. Hasan, M. Dilshad, A. Zafar, T. Tariq, A. Shaheen, R. Iqbal, Z. Ali, T. Munawar, F. Iqbal, S.G. Hassan, X. Shu, G. Caprioli, Green synthesized ZnO-Fe_2O_3-Co_3O_4 nanocomposite for antioxidant, microbial disinfection and degradation of pollutants from wastewater, Biochem. Syst. Ecol. 105 (2022) 104535.

[28] F. Mukhtar, T. Munawar, M.S. Nadeem, M.Nu Rehman, M. Riaz, F. Iqbal, Dual S-scheme heterojunction ZnO–V_2O_5–WO_3 nanocomposite with enhanced photocatalytic and antimicrobial activity, Mater. Chem. Phys. 263 (2021) 124372.

[29] Y. Wang, X.-y Yang, Z.-q Lai, G. Li, Zn.O.-Loaded Ion, Exchange resin composites: preparation, characterization and photocatalytic application, Environ. Eng. Sci. 41 (2024) 131–139.

[30] K. Mubeen, K. Safeen, A. Irshad, A. Safeen, T. Ghani, W.H. Shah, R. Khan, K. S. Ahmad, R. Casin, M.A. Rashwan, H.O. Elansary, A. Shah, ZnO/CuSe composite-mediated bandgap modulation for enhanced photocatalytic performance against methyl blue dye, Sci. Rep. 13 (2023) 19580.

[31] M.M. Khan, S.F. Adil, A. Al-Mayouf, Metal oxides as photocatalysts, J. Saudi Chem. Soc. 19 (2015) 462–464.

[32] A. Akkaya, E. Ayyıldız, Automation software for semiconductor research laboratories: electrical parameter calculation program (SeCLaS-PC), J. Circuits, Syst. Comput. 29 (2020) 2050215.

[33] S. Harish, J. Archana, M. Sabarinathan, M. Navaneethan, K.D. Nisha, S. Ponnusamy, C. Muthamizhchelvan, H. Ikeda, D.K. Aswal, Y. Hayakawa, Controlled structural and compositional characteristic of visible light active ZnO/CuO photocatalyst for the degradation of organic pollutant, Appl. Surf. Sci. 418 (2017) 103–112.

[34] T. Munawar, F. Iqbal, S. Yasmeen, K. Mahmood, A. Hussain, Multi metal oxide NiO-CdO-ZnO nanocomposite–synthesis, structural, optical, electrical properties and enhanced sunlight driven photocatalytic activity, Ceram. Int. 46 (2020) 2421–2437.

[35] J.-M. Herrmann, Heterogeneous photocatalysis: fundamentals and applications to the removal of various types of aqueous pollutants, Catal. Today 53 (1999) 115–129.

[36] S. Xia, L. Zhang, G. Pan, P. Qian, Z. Ni, Photocatalytic degradation of methylene blue with a nanocomposite system: synthesis, photocatalysis and degradation pathways, Phys. Chem. Chem. Phys. 17 (2015) 5345–5351.

[37] R. Aydın, A. Akkaya, B. Şahin, Light-weight and flexible Ni-doped CuO (Ni:CuO) thin films grown using the cost-effective SILAR method for future technological requests, J. Mater. Sci.: Mater. Electron. 33 (2022) 23806–23820.

[38] Z.N. Ozer, M. Ozkan, S. Pat, Optical and electric characteristics of CuO nanoparticle-doped ZnO thin films using thermionic vacuum arc deposition system, J. Mater. Sci.: Mater. Electron. 35 (2024) 456.

[39] N.S. Kirik, B. Şahin, Characteristics modification of ZnO/CuO composite films by doping rare-earth element Dy for real-time hydration level monitoring, Micro Nanostruct. 167 (2022) 207290.

[40] T. Munawar, S. Yasmeen, F. Hussain, K. Mahmood, A. Hussain, M. Asghar, F. Iqbal, Synthesis of novel heterostructured ZnO-CdO-CuO nanocomposite: Characterization and enhanced sunlight driven photocatalytic activity, Mater. Chem. Phys. 249 (2020) 122983.

[41] S.P. Adhikari, H.R. Pant, J.H. Kim, H.J. Kim, C.H. Park, C.S. Kim, One pot synthesis and characterization of Ag-ZnO/g-C_3N_4 photocatalyst with improved photoactivity and antibacterial properties, Colloids Surf. A: Physicochem. Eng. Asp. 482 (2015) 477–484.

[42] A.S. Beheshtian, M.H. Givianrad, H.-A. Rafiee-Pour, P.A. Azar, Malva sylvestris mediated synthesis of CuO NPs towards electrochemical determination of quercetin, Opt. Quant. Electron 55 (2023) 463.

[43] M. Bououdina, A.A. Dakhel, M. El-Hilo, D.H. Anjum, M.B. Kanoun, S. Goumri-Said, Revealing a room temperature ferromagnetism in cadmium oxide nanoparticles: an experimental and first-principles study, RSC Adv. 5 (2015) 33233–33238.

[44] M.T. Maru, B.A. Gonfa, O.A. Zelekew, S.P. Fakrudeen, H.C. Ananda Murthy, E. T. Bekele, F.K. Sabir, Effect of Musa acuminata peel extract on synthesis of ZnO/CuO nanocomposites for photocatalytic degradation of methylene blue, Green. Chem. Lett. Rev. 16 (2023) 2232383.

[45] A. Khalid, P. Ahmad, A. Khan, A.A.H. Abdellatif, A.M. Abu-Dief, B.S. Al-Anzi, H. A. Almukhlifi, H.W. Alhamdi, A.M. Alanazi, O.A. Jefri, M.M. Alsowayigh, A. H. Alsehli, S.A. Alderhami, R. Ahmed, Development of CuO and CuO:Zn^{2+} nano-oxides for dye degradation and pharmaceutical studies, Inorg. Chem. Commun. 160 (2024) 111887.

[46] B. Karthikeyan, R. Vettumperumal, Optical and electrochemical properties of pure and Ti-doped CdO nanoparticles for device applications, Mater. Sci. Eng.: B 281 (2022) 115754.

[47] R. Aydın, A. Akkaya, O. Kahveci, B. Şahin, Nanostructured CuO thin-film-based conductometric sensors for real-time tracking of sweat loss, ACS Omega 8 (2023) 20009–20019.

[48] O. Kahveci, A. Akkaya, R. Aydın, B. Şahin, E. Ayyıldız, Synthesis of Al and In dual-doped CuO nanostructures via SILAR method: structural, optical and electrical properties, Inorg. Chem. Commun. 147 (2023) 110230.

[49] T. Munawar, F. Mukhtar, M.S. Nadeem, S. Manzoor, M.N. Ashiq, K. Mahmood, S. Batool, M. Hasan, F. Iqbal, Fabrication of dual Z-scheme TiO_2-WO_3-CeO_2 heterostructured nanocomposite with enhanced photocatalysis, antibacterial, and electrochemical performance, J. Alloy Compd. 898 (2022) 162779.

[50] M.Z. Ishaque, Y. Zaman, A. Arif, A.B. Siddique, M. Shahzad, D. Ali, M. Aslam, H. Zaman, M. Faizan, Fabrication of ternary metal oxide (ZnO:NiO:CuO) nanocomposite heterojunctions for enhanced photocatalytic and antibacterial applications, RSC Adv. 13 (2023) 30838–30854.

[51] H. Satılmış, M. Acar, R. Aydın, A. Akkaya, O. Kahveci, B. Şahin, E. Ayyıldız, Cd-supported CuO-ZnO binary oxide thin films: synthesis, microstructural, and optoelectronic properties, Opt. Mater. 148 (2024) 114851.

[52] Y. Zaman, M.Z. Ishaque, K. Waris, M. Shahzad, A.B. Siddique, M.I. Arshad, H. Zaman, H.M. Ali, F. Kanwal, M. Aslam, M. Mustaqeem, Modified physical properties of Ni doped ZnO NPs as potential photocatalyst and antibacterial agents, Arab J. Chem. 16 (2023) 105230.

[53] R. Keuleers, H.O. Desseyn, B. Rousseau, C. Van Alsenoy, Vibrational analysis of urea, J. Phys. Chem. A 103 (1999) 4621–4630.

[54] M.M. El-Desoky, M.A. Ali, G. Afifi, H. Imam, M.S. Al-Assiri, Effects of annealing temperatures on the structural and dielectric properties of ZnO nanoparticles, Silicon 10 (2018) 301–307.

[55] H. Singh, K.L. Yadav, Structural, dielectric, vibrational and magnetic properties of Sm doped $BiFeO_3$ multiferroic ceramics prepared by a rapid liquid phase sintering method, Ceram. Int 41 (2015) 9285–9295.

[56] K.A. Khan, A. Shah, J. Nisar, A. Haleem, I. Shah, Photocatalytic degradation of food and juices dyes via photocatalytic nanomaterials synthesized through green synthetic route: a systematic review, Molecules 28 (2023) 4600.

[57] B. Dong, X. Yu, Z. Dong, X. Yang, Y. Wu, Facile synthesis of ZnO nanoparticles for the photocatalytic degradation of methylene blue, J. Sol. -Gel Sci. Techn. 82 (2017) 167–176.

[58] F. Acartürk, I. Agabeyoglu, N. Celebi, T. Degim, Z. Degim, T. Doğanay, S. Takka, F. TırnaksızReaction Kinetics and Stability, in: In Modern Pharmaceutical Technology, Turkish Pharmacists Association Pharmacy Academy Publication, 2009, pp. 141-182.2009, , 141–182..

[59] N. Serpone, D. Lawless, R. Khairutdinov, E. Pelizzetti, Subnanosecond relaxation dynamics in TiO2 colloidal sols (particle sizes Rp = 1.0–13.4 nm). Relevance to heterogeneous photocatalysis, J. Phys. Chem. 99 (1995) 16655–16661.

[60] F. Amano, E. Ishinaga, A. Yamakata, Effect of particle size on the photocatalytic activity of WO_3 particles for water oxidation, J. Phys. Chem. C 117 (2013) 22584–22590.

[61] C.B. Almquist, P. Biswas, Role of synthesis method and particle size of nanostructured TiO_2 on its photoactivity, J. Catal. 212 (2002) 145–156.

[62] B. Li, Y. Wang, Facile synthesis and photocatalytic activity of ZnO–CuO nanocomposite, Superlattice Microstruct. 47 (2010) 615–623.

[63] P. Bharathi, S. Harish, J. Archana, M. Navaneethan, S. Ponnusamy, C. Muthamizhchelvan, M. Shimomura, Y. Hayakawa, Enhanced charge transfer and separation of hierarchical CuO/ZnO composites: the synergistic effect of photocatalysis for the mineralization of organic pollutant in water, Appl. Surf. Sci. 484 (2019) 884–891.

[64] C.V. Reddy, B. Babu, J. Shim, Synthesis, optical properties and efficient photocatalytic activity of CdO/ZnO hybrid nanocomposite, J. Phys. Chem. Solids 112 (2018) 20–28.

[65] U. Farooq, T. Ahmad, F. Naaz, Su Islam, Review on metals and metal oxides in sustainable energy production: progress and perspectives, Energy Fuels 37 (2023) 1577–1632.

[66] A.H. Bhat, H.-T.-N. Chisti, Facile fabrication of ternary metal oxide ZnO/CuO/SnO_2 nanocomposite for excellent photocatalytic degradation of fast green dye, Int. J. Environ. Anal. Chem. 103 (2023) 9594–9615.

[67] A. Doyan, L. Susilawati, S. Muliyadi, H. Hakim, M. Munandar, Taufik, The effect of dopant material to optical properties: energy band gap Tin Oxide thin film, J. Phys.: Conf. Ser. 1816 (2021) 012114.

[68] Y. Rajesh, S.K. Padhi, M.G. Krishna, ZnO thin film-nanowire array homo-structures with tunable photoluminescence and optical band gap, RSC Adv. 10 (2020) 25721–25729.

[69] R. Aydın, B. Şahin, The role of Triton X-100 as a surfactant on the CdO nanostructures grown by the SILAR method, J. Alloy Compd. 705 (2017) 9–13.

[70] K. Yousra, E. Guettaf Temam, R. Saâd, H. Barkat, Effect of film thickness on the electrical and the photocatalytic properties of ZnO nanorods grown by SILAR technique, Phys. Scr. 98 (2023) 125954.

[71] B. Gokul, P. Matheswaran, R. Sathyamoorthy, Influence of annealing on physical properties of CdO thin films prepared by SILAR method, J. Mater. Sci. Technol. 29 (2013) 17–21.

[72] C.J. Kevane, Oxygen vacancies and electrical conduction in metal oxides, Phys. Rev. 133 (1964) A1431–A1436.

[73] M. Anwar, S.A. Siddiqi, I.M. Ghauri, Ac conduction in mixed oxides Al-In_2O_3-SnO_2-Al structure deposited by co-evaporation, Surf. Rev. Lett. 13 (2006) 457–469.

[74] O. Kahveci, A. Akkaya, E. Yücel, R. Aydın, B. Şahin, Production of p-CuO/n-ZnO:Co nanocomposite heterostructure thin films: an optoelectronic study, Ceram. Int. 49 (2023) 16458–16466.

[75] D.K. Schroder, Semiconductor Material And Device Characterization, John Wiley & Sons, New York, 2006.
[76] H. Murrmann, D. Widmann, Current crowding on metal contacts to planar devices, IEEE Trans. Electron Devices 16 (1969) 1022–1024.
[77] R.R. Salunkhe, D.S. Dhawale, T.P. Gujar, C.D. Lokhande, Structural, electrical and optical studies of SILAR deposited cadmium oxide thin films: annealing effect, Mater. Res. Bull. 44 (2009) 364–368.